Plant, Cell & Environment

Plant, Cell and Environment (2017) **40**, 1618–1628 doi: 10.1111/pce.12970

Original Article

Stomatal kinetics and photosynthetic gas exchange along a continuum of isohydric to anisohydric regulation of plant water status

Frederick C. Meinzer[1], Duncan D. Smith[2], David R. Woodruff[1], Danielle E. Marias[3], Katherine A. McCulloh[3], Ava R. Howard[4] & Alicia L. Magedman[3]

[1]*Pacific Northwest Research Station, USDA Forest Service, Corvallis, OR 97331, USA,* [2]*Department of Botany, University of Wisconsin, Madison, WI 53706, USA,* [3]*Department of Forest Ecosystems and Society, Oregon State University, Corvallis, OR 97331, USA and* [4]*Department of Biology, Western Oregon University, Monmouth, OR 97361, USA*

ABSTRACT

Species' differences in the stringency of stomatal control of plant water potential represent a continuum of isohydric to anisohydric behaviours. However, little is known about how quasi-steady-state stomatal regulation of water potential may relate to dynamic behaviour of stomata and photosynthetic gas exchange in species operating at different positions along this continuum. Here, we evaluated kinetics of light-induced stomatal opening, activation of photosynthesis and features of quasi-steady-state photosynthetic gas exchange in 10 woody species selected to represent different degrees of anisohydry. Based on a previously developed proxy for the degree of anisohydry, species' leaf water potentials at turgor loss, we found consistent trends in photosynthetic gas exchange traits across a spectrum of isohydry to anisohydry. More anisohydric species had faster kinetics of stomatal opening and activation of photosynthesis, and these kinetics were closely coordinated within species. Quasi-steady-state stomatal conductance and measures of photosynthetic capacity and performance were also greater in more anisohydric species. Intrinsic water-use efficiency estimated from leaf gas exchange and stable carbon isotope ratios was lowest in the most anisohydric species. In comparisons between gas exchange traits, species rankings were highly consistent, leading to species-independent scaling relationships over the range of isohydry to anisohydry observed.

Key-words: anisohydry; intrinsic water-use efficiency; photosynthesis; turgor.

INTRODUCTION

The stringency with which stomata regulate plant water status has implications for balancing plant carbon gain with water loss, especially during periods of drought. The so-called isohydric species exhibit stringent control of daily minimum leaf water potential (Ψ_{min}) as soil water potential (Ψ_{soil}) declines, whereas stomata in anisohydric species allow Ψ_{min} to decline in concert with Ψ_{soil} (Tardieu & Simonneau 1998; Franks *et al.* 2007; Klein 2014; Martínez-Vilalta *et al.* 2014). However, rather than representing dichotomous modes of stomatal regulation, isohydry versus anisohydry represent extremes of a continuum of stringency of stomatal control of leaf Ψ as Ψ_{soil} varies (Meinzer *et al.* 2016). Where species operate along this continuum may have implications for the principal mechanisms driving drought-induced plant mortality. Isohydric species have been hypothesized to be at greater risk of death from depletion of carbohydrate reserves during prolonged drought because their stomata generally close at less negative values of Ψ_{soil} (McDowell *et al.* 2008, 2011). Although results of some studies are consistent with this hypothesis (Mitchell *et al.* 2013), other studies conducted under multiyear drought conditions have found evidence for hydraulic dysfunction, but not depletion of carbohydrate reserves in isohydric species (Anderegg *et al.* 2012), or greater mortality in an isohydric species than in an anisohydric species in a common garden experiment, despite similar carbohydrate dynamics and similar, mild levels of hydraulic dysfunction in both species (Garcia-Forner *et al.* 2016a).

Because of its potential implications for plant performance and survival during drought, there has been intense interest in quantitatively ranking species according to their degree of isohydry–anisohydry (McDowell *et al.* 2011; Martínez-Vilalta *et al.* 2014; Martínez-Vilalta & Garcia-Forner 2016). Attempts to position species along a continuum of isohydry to anisohydry have generally relied upon labour-intensive measurements of stomatal conductance and plant and soil water potentials during prolonged soil drying cycles (Ewers *et al.* 2007; West *et al.* 2007; Skelton *et al.* 2015; Garcia-Forner *et al.* 2016b). However, rankings of species may differ according to the types of metrics of stringency of stomatal control of Ψ_{min} derived from these data sets (Klein 2014; Martinez-Vilalta & Garcia-Forner 2016). Recently, leaf pressure–volume traits of well-watered plants were shown to be robust proxies for stringency of stomatal control of Ψ_{min} during subsequent soil drying (Meinzer *et al.* 2016). Among eight woody species, leaf osmotic potentials at full and zero turgor were strong predictors of

Correspondence: F. C. Meinzer; e-mail: rick.meinzer@oregonstate.edu; fmeinzer@fs.fed.us

species' 'hydroscapes', or water potential landscapes over which stomata were able to regulate leaf gas exchange and plant water status prior to permanent drought-induced stomatal closure. Larger hydroscapes and more negative osmotic potentials were indicative of more anisohydric behavior (Meinzer *et al.* 2016). These leaf pressure–volume traits were also strong predictors of the rate at which stomata constrained daily variation in leaf water potential as soil water potential declined. The ability of leaf pressure–volume traits to serve as proxies for different metrics of stomatal behaviour during soil drying is likely related to the mechanistic dependence of stomatal conductance on bulk leaf and guard cell turgor (Raschke 1975; Buckley 2005; Rodriguez-Dominguez *et al.* 2016).

Our understanding of how complexes of plant functional traits are coordinated along the continuum of isohydry to anisohydry is limited in part because species' rankings can vary according to the criteria applied in a given study. Nevertheless, traits associated with regulation of plant water balance and maintenance of xylem water transport likely involve trade-offs that conform with resource economics spectra described for leaves (Wright *et al.* 2004) and whole plants (Reich 2014). Because stomatal regulation of leaf Ψ serves to avoid hydraulic dysfunction in stems upstream from leaves (Sparks & Black 1999; Meinzer *et al.* 2009), anisohydric species tend to have more embolism-resistant xylem in their stems than do isohydric species (Vogt 2001; McDowell *et al.* 2008; Skelton *et al.* 2015). More embolism-resistant xylem is often, but not always, associated with higher wood density (Hacke *et al.* 2001; Pratt *et al.* 2007a; Bucci *et al.* 2013). Increasing wood density along a spectrum of isohydry to anisohydry may imply further trade-offs against other xylem water transport properties such as hydraulic conductivity and capacitance (Bucci *et al.* 2004; Scholz *et al.* 2007; Meinzer *et al.* 2008). The tendency for anisohydric species to operate at larger hydraulic safety margins than isohydric species when soil water availability is adequate (Meinzer *et al.* 2009; Garcia-Forner *et al.* 2016b) may be associated with their lower hydraulic capacitance and therefore reduced ability to buffer dynamic fluctuations in xylem pressure. Although Ψ_{min} in isohydric and anisohydric species is often regarded as a quasi-steady-state response to gradual changes in Ψ_{soil}, stomata must regulate transpiration and plant water status dynamically in response to sometimes rapid fluctuations in atmospheric variables such as vapour pressure deficit (VPD).

Given the preceding considerations and the close coordination between vapour and liquid-phase water transport properties (Meinzer & Grantz 1990; Hubbard *et al.* 2001; Meinzer 2002), we expect that trade-offs associated with variation in biophysical traits and constraints along a continuum of isohydry to anisohydry will be reflected in both dynamic and quasi-steady-state stomatal responses to fluctuating environmental variables. Specifically, in plants experiencing adequate water availability, we expect faster stomatal kinetics and higher quasi-steady-state stomatal conductance (g_s) along a continuum of increasing anisohydry. Additionally, in view of the inextricable link between stomatal behaviour and photosynthetic CO_2 uptake, we also expect stomatal and photosynthetic traits to co-vary along this continuum. Thus, if stomatal kinetics are faster and g_s higher in more anisohydric species, we expect faster activation and higher maximum rates of photosynthesis with increasing anisohydry when isohydric and anisohydric species are held under comparable conditions of minimal water stress. We addressed these expectations by characterizing several features of dynamic and quasi-steady-state regulation of photosynthetic gas exchange in well-irrigated individuals of 10 diverse woody species representing a broad range of isohydric to anisohydric behaviours based on their bulk leaf osmotic properties as determined from pressure–volume curves (Meinzer *et al.* 2016). We quantified absolute and relative rates of light-induced stomatal opening and activation of photosynthesis, quasi-steady-state operating stomatal conductance, CO_2 assimilation rates, various measures of photosynthetic capacity and intrinsic water-use efficiency (WUE).

MATERIALS AND METHODS

Plant material and growing conditions

Analyses were conducted on 10 woody species selected based on two criteria: (1) stringency of stomatal control inferred from the literature (i.e. species' ecological distributions and ecophysiological traits) and (2) their availability at a local nursery (Sevenoaks Native Nursery, Albany, OR, USA). The species (Table 1) are characteristic of a spectrum of vegetation types, including chaparral, oak woodland, sagebrush scrub and forest. In March 2015, ten 1- to 2-year-old plants of each species were transplanted from their original containers to 9.8-L pots containing a 1:1 mixture of commercial potting mix (Metro-mix 840, Sun Gro Horticulture, Agawam, MA, USA) and sandy loam soil. Plants were grown in a climate-controlled greenhouse on the Oregon State University campus, and all pots were irrigated to drainage daily prior to and throughout the measurement period, which spanned from late June to early July. These experimental conditions were imposed to increase our ability to characterize inherent photosynthetic gas exchange traits associated with species' operating positions along a continuum of isohydry to anisohydry and to minimize the influence of potentially confounding factors such as rooting depth and rate and severity of soil drying. Maximum photosynthetically active radiation (PAR) inside the greenhouse was ~800 μmol m^{-2} s^{-1}, average relative humidity was ~71% and average air temperature was ~20 °C. Plant dimensions measured in August are shown in Supporting Information Table S1.

Positioning of species along a continuum of isohydry to anisohydry

Procedures for using species' leaf pressure–volume curve traits as proxies for quantifying stringency of stomatal control of plant water status during soil drying are described in detail by Meinzer *et al.* (2016). Briefly, the bulk leaf water (and osmotic) potential at the turgor loss point (Ψ_{TLP}) was found to be a

Table 1. Bulk leaf water potential at the turgor loss point (Ψ_{TLP} ± SE) and other characteristics of the 10 woody species in which stomatal kinetics and photosynthetic gas exchange were characterized

Species	Code	Family	Life form	Leaf phenology	Ψ_{TLP} (MPa)
Alnus incana	ALIN	Betulaceae	Tree	Deciduous	−1.32 ± 0.05
Betula occidentalis	BEOC	Betulaceae	Shrub/tree	Deciduous	−1.37 ± 0.07
Sambucus racemosa	SARA	Adoxaceae	Shrub/tree	Deciduous	−1.41 ± 0.03
Salix scouleriana	SASC	Salicaceae	Shrub/tree	Deciduous	−1.88 ± 0.04
Heteromeles arbutifolia	HEAR	Rosaceae	Shrub	Evergreen	−2.26 ± 0.04
Cercocarpus ledifolius	CELE	Rosaceae	Shrub/tree	Evergreen	−2.31 ± 0.09
Rhamnus ilicifolia	RHIL	Rhamnaceae	Shrub	Evergreen	−2.39 ± 0.01
Quercus garryana	QUGA	Fagaceae	Tree	Deciduous	−2.62 ± 0.08
Quercus douglasii	QUDO	Fagaceae	Tree	Deciduous	−2.65 ± 0.04
Ceanothus cuneatus	CECU	Rhamnaceae	Shrub	Evergreen	−2.89 ± 0.05

Species are arranged in order of increasing anisohydry.

robust proxy for two metrics of species' degree of anisohydry: (1) a 'hydroscape' or Ψ landscape over which stomata were effectively able to regulate leaf Ψ prior to complete drought-induced stomatal closure and cessation of photosynthetic gas exchange and (2) the steepness with which the difference between pre-dawn and daily minimum Ψ (ΔΨ) diminished with declining pre-dawn Ψ (Ψ_{pd}) during soil drying. According to these metrics, more anisohydric species show larger hydroscape areas and smaller declines in ΔΨ with declining Ψ_{pd}. Increasingly negative species' Ψ_{TLP} were predictive of larger hydroscape areas (r^2 = 0.93, P = 0.0001) and smaller declines in ΔΨ with declining Ψ_{pd} (r^2 = 0.80, P = 0.004). Use of Ψ_{TLP} as a proxy for positioning species along a continuum of isohydry to anisohydry has mechanistic underpinnings because loss of leaf turgor represents the limit for sustaining stomatal opening and gas exchange. Values of Ψ_{TLP} for the 10 species in the current study (Table 1) were determined during the period when leaf gas exchange traits were being characterized (June–July) and represent means of pressure–volume curves from three to five individuals. In contrast, values of Ψ_{TLP} reported by Meinzer *et al.* (2016) represent seasonal means (June–September) for irrigated plants and did not include *Alnus incana* and *Sambucus racemosa*, which were not subjected to the soil drying treatment implemented in August in our prior study.

Leaf gas exchange

Plants were transported from the greenhouse to the nearby laboratory during the afternoon to allow them to become dark adapted prior to gas exchange measurements the following morning. PAR from ceiling fluorescent lights in the windowless laboratory was 3–5 μmol m^{-2} s^{-1} at plant height. For measurements of rates of light-induced stomatal opening and activation of photosynthesis, we followed a protocol similar to that described by Drake *et al.* (2013). All measurements were made with portable photosynthetic gas exchange systems (LI-6400, Li-Cor, Lincoln, NE, USA) and were typically initiated between 0800 and 0900 h. Measurements were initiated by first sealing a portion of a leaf or leaves in the darkened gas exchange cuvette and then automatically logging values of stomatal conductance (g_s), net CO_2 exchange (A) and cuvette environmental parameters every 120 s until g_s remained nearly stable for three or more measurements. A data logging interval of 120 s was selected because it was the minimum amount of time necessary to accommodate the infrared gas analyser's automated CO_2 and water vapour matching function performed prior to logging each data point. The value of g_s at this point was denoted as the minimum g_s under the dark adaptation conditions imposed ($g_{s\ dark}$, Fig. 1). The light-emitting diode light source in the cuvette was then set at PAR = 1200 μmol m^{-2} s^{-1}, and logging of data every 120 s continued until light-induced stomatal opening and activation of photosynthesis were essentially complete. Attainment of operating stomatal conductance under the conditions imposed was judged on the basis of g_s having

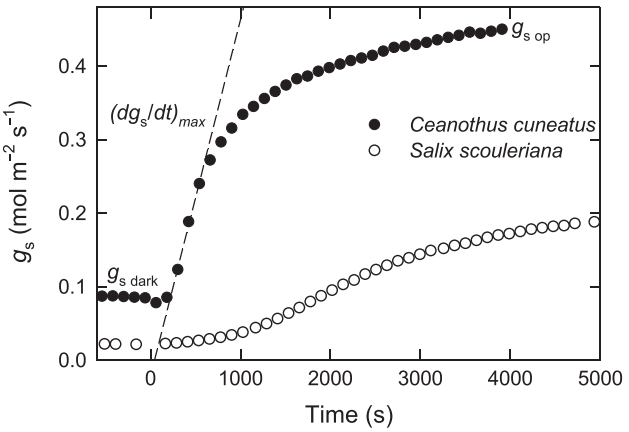

Figure 1. Sample time courses of light-induced stomatal opening in dark-adapted leaves of two woody species representing different operating points along a continuum of isohydric to anisohydric regulation of plant water status. Parameters derived from the time courses are stomatal conductance of dark-adapted leaves ($g_{s\ dark}$), maximum rate of light-induced stomatal opening [$(dg_s/dt)_{max}$] and quasi-steady-state operating conductance in the light ($g_{s\ op}$). Leaves were illuminated at time = 0. Based on its leaf turgor loss point, *Ceanothus cuneatus* is more anisohydric than *Salix scouleriana*. Only parameters for *C. cuneatus* are shown for simplicity. See text for further details.

approached an asymptote ($g_{s\ op}$, Fig. 1), and full activation of photosynthesis was considered to have occurred when the ratio of A to intercellular [CO_2] (C_i) became essentially constant (Supporting Information Fig. S1). During these time courses, leaf temperature was maintained at 25 °C and reference [CO_2] at 400 μmol mol^{-1}. Because of variation between measurements in amounts of leaf area in the cuvette and variation in species values of $g_{s\ dark}$ and $g_{s\ op}$, it was not feasible to maintain a constant leaf-to-air VPD in the cuvette within a measurement time course (cf., Drake *et al.* 2013). Instead, VPD was minimized by maintaining a low gas exchange system flow rate while bypassing the desiccant. Mean values of VPD (±SE) were 1.56 ± 0.04 and 1.07 ± 0.04 kPa at the times $g_{s\ dark}$ and $g_{s\ op}$ were determined, respectively. Values of VPD at the times $g_{s\ dark}$ and $g_{s\ op}$ were determined were not significantly correlated with species' values of Ψ_{TLP} (P = 0.95 and 0.72, respectively), our proxy for degree of anisohydry. The preceding measurements were made on four to five individuals of each species.

Once light-induced stomatal opening and activation of photosynthesis were complete, the response of A to C_i was characterized. Measurements began near ambient [CO_2] (C_a) of 400 μmol mol^{-1}, and C_a was reduced in steps to 50 μmol mol^{-1} and then raised directly to 400 μmol mol^{-1} for a repeated measurement and raised further in steps to 2000 to 2100 μmol mol^{-1}. The resulting A–C_i curves consisted of 9 to 11 points. Maximum rates of photosynthesis at PAR = 1200 μmol m^{-2} s^{-1} (A_{max}) were estimated as the asymptote of a function fitted to the data. The maximum rate of carboxylation ($V_{c\ max}$) and the maximum rate of electron transport at PAR = 1200 μmol m^{-2} s^{-1} (J_{1200}) were estimated from the A–C_i curve data using the spreadsheet utility developed by Sharkey *et al.* (2007).

Leaf δ^{13}C, N content and leaf mass per area

The leaves on which photosynthetic gas exchange had been measured were dried and ground to a fine powder for δ^{13}C analyses. These leaves had been selected on the basis of their being as fully exposed as possible to the ambient light conditions in the greenhouse and experiencing minimal shading by other leaves and plants. δ^{13}C analyses were conducted at the stable isotope laboratory in the College of Earth, Oceanic and Atmospheric Sciences at Oregon State University. The samples were combusted in an elemental analyser (Carlo Erba NA 1500, Thermo Scientific, Waltham, MA, USA), and the resulting CO_2 was analysed by a continuous-flow isotope ratio mass spectrometer (Delta Plus XL, Thermo Scientific). Runs were calibrated using the international standards USGS40 glutamic acid and SIL sucrose. The typical error was ±0.1‰ or better as determined by repeated measures of internal quality control standards (IAEA-600 caffeine) and from sample replicates. The same analyses yielded leaf N content on a dry mass basis. For leaf mass per area (LMA), freshly collected leaves were scanned to determine their area, and then their dry mass was determined after drying at least 24 h in a 70 °C oven. Values of LMA for *S. racemosa* were not available because it was discovered after conclusion of the experiment that leaf area scanning and dry mass determination had not been conducted for this species.

Analyses

The maximum rate of light-induced stomatal opening [$(dg_s/dt)_{max}$] was estimated from the slope of a linear regression fitted to the steepest portion of the time course of g_s after PAR in the gas exchange cuvette was set at 1200 μmol m^{-2} s^{-1} (Fig. 1). Selection of data points was guided by the criterion of maximizing the r^2 value for a linear fit when more than two data points were included. The asymptote of a function fitted to the time course of g_s from the first point used to estimate $(dg_s/dt)_{max}$ to the last data point collected was used to estimate $g_{s\ op}$. The procedure for estimating the maximum rate of light-induced activation of photosynthesis was similar to that used for $(dg_s/dt)_{max}$, except that instead of using absolute rates of photosynthesis, which were constrained by g_s, time courses of A/C_i (e.g. Supporting Information Fig. S1) were used for fitting regressions to the steepest portions of the time courses. Regression slopes were then normalized by assigning a value of 1 to the steepest species mean slope, yielding a dimensionless estimate of relative rates of activation of photosynthesis across species. The preceding linear regression approach was used because visual inspection of time courses indicated maximum rates were consistently underestimated when various types of sigmoid functions were fitted to the data. The kinetics of light-induced stomatal opening and activation of photosynthesis were also analysed in terms of times required to reach 50% of their final quasi-steady-state values (half-times; $t_{50\ gs}$, $t_{50\ A}$) to address the possibility of autocorrelation between absolute rates and maximum steady-state values.

Significance of relationships between variables was evaluated from Spearman's rank correlation coefficients because many of the relationships were obviously non-linear and we were interested in assessing consistency of species rankings as they related to their degree of anisohydry. Thus, significance levels reported in the figures and text represent those for Spearman's r values. Functions fitted to the data in the figures were either least squares linear regressions or non-linear functions that provided the best fits. Means and standard errors for the variables plotted in Figs 2–10 are shown in Supporting Information Table S2.

RESULTS

Stomatal conductance traits characterized during light-induced stomatal opening experiments varied broadly across the 10 species studied (Figs 1 & 2). The maximum rate of light-induced stomatal opening [$(dg_s/dt)_{max}$] ranged from 0.017 mmol m^{-2} s^{-2} in *S. racemosa* to 0.441 mmol m^{-2} s^{-2} in *Ceanothus cuneatus* and was strongly correlated with interspecific variation in the quasi-steady-state operating stomatal conductance ($g_{s\ op}$) in the light (Fig. 2a). However, the relative variation in $(dg_s/dt)_{max}$ across species was about four times greater than that of $g_{s\ op}$. Stomatal conductance prior to illumination of leaves in the gas

exchange cuvette ($g_{s\ dark}$) was significantly correlated with $g_{s\ op}$ across species (Fig. 2b), but the correlation was weaker than that between $g_{s\ op}$ and $(dg_s/dt)_{max}$. Faster stomatal kinetics and higher operating conductance were associated with higher species' maximum bulk leaf turgor at full hydration estimated from pressure–volume curves (Fig. 3).

The preceding stomatal conductance traits varied with species' positions along a continuum of isohydric to anisohydric regulation of plant water status as estimated from leaf water potential at the turgor loss point (Ψ_{TLP}), which ranged from −1.32 MPa in the more isohydric *A. incana* to −2.89 MPa in the more anisohydric *C. cuneatus* (Table 1). The maximum rate of light-induced stomatal opening and the operating stomatal conductance in the light increased with greater anisohydry across species (Fig. 4a,b). Minimum g_s of dark-adapted leaves also increased with increasing anisohydry, but the relationship was not as strong as that observed for $g_{s\ op}$ and $(dg_s/dt)_{max}$ largely because of data obtained for *Cercocarpus ledifolius* (Fig. 4c).

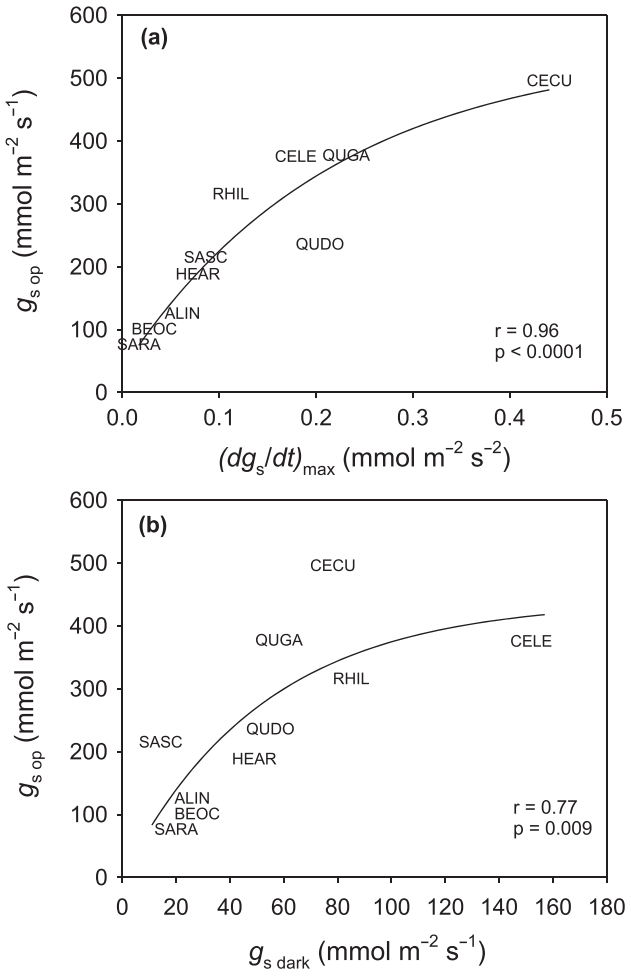

Figure 2. Relationships between stomatal conductance parameters in light-induced stomatal opening experiments. Operating conductance ($g_{s\ op}$) in relation to (a) the maximum rate of stomatal opening [$(dg_s/dt)_{max}$] and (b) steady-state conductance of dark-adapted leaves ($g_{s\ dark}$). See Fig. 1 for derivation of parameters and Table 1 for species abbreviations.

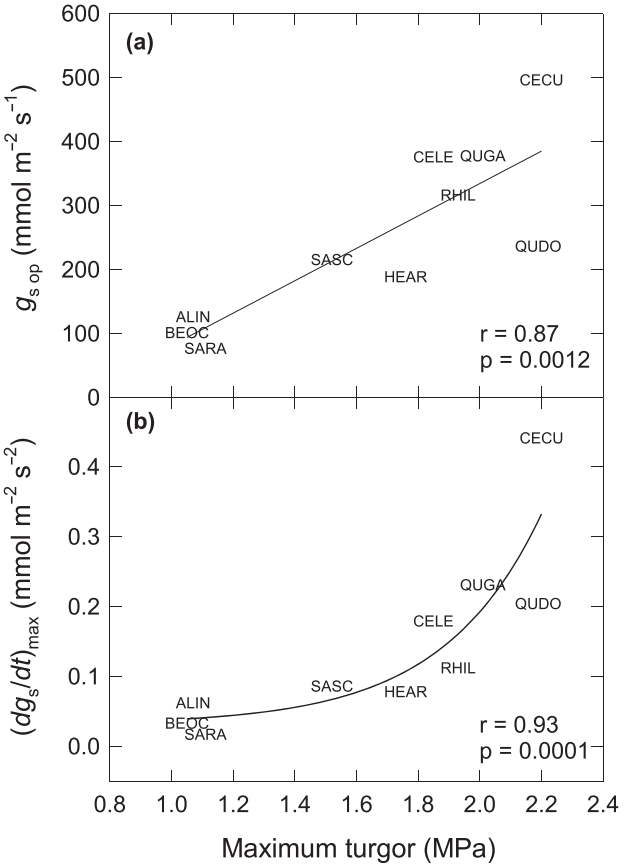

Figure 3. Stomatal conductance parameters in light-induced stomatal opening experiments in relation to maximum turgor in fully hydrated leaves (i.e. $-\Psi_{\pi\ 100}$ if leaf $\Psi = 0$). See Fig. 1 for derivation of stomatal conductance parameters and Table 1 for species abbreviations.

Consistent with stomatal conductance traits, several metrics of species' photosynthetic performance were strongly associated with their degree of anisohydry (Fig. 5). The relative rate of light-induced photosynthetic activation was about five times higher in the species with the most negative value of Ψ_{TLP}, *C. cuneatus*, than that in *Betula occidentalis* and *S. racemosa* whose values of Ψ_{TLP} were about 1.5 MPa less negative (Fig. 5a). However, the maximum relative rate of activation of photosynthesis was roughly three times greater in *A. incana* than in similarly isohydric *B. occidentalis* and *S. racemosa*. Leaf nitrogen content in *A. incana* (3%), which was observed to have nodulated roots, indicating the likely presence of nitrogen-fixing bacteria, was about 75% greater than that in *B. occidentalis* (N = 1.6%) and *S. racemosa* (N = 1.8%). However, leaf N content on an area basis (N_{area}) was similar among the three species (Fig. 6b). Removal of *A. incana* from the analysis substantially increased the strength of the relationship between photosynthetic induction rates and leaf turgor loss points ($r = -0.91$, $P = 0.0006$). Three metrics of quasi-steady-state photosynthetic performance, A_{max}, $V_{c\ max}$ and J_{1200}, also increased with increasing anisohydry as estimated from species' turgor loss points (Fig. 5b,c,d). For these three quasi-steady-state metrics, the behavior of *A. incana* was similar

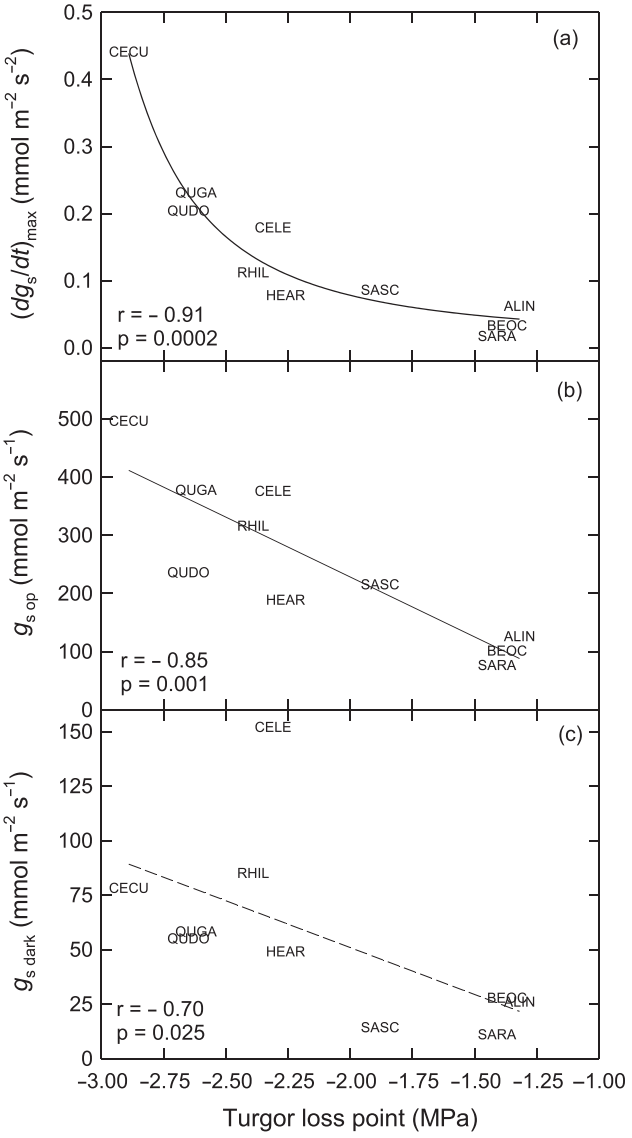

Figure 4. Stomatal conductance parameters in light-induced stomatal opening experiments in relation to leaf water potential at the turgor loss point. More negative values of the turgor loss point have been associated with more anisohydric stomatal regulation of leaf water potential. See Fig. 1 for derivation of stomatal conductance parameters and Table 1 for species abbreviations.

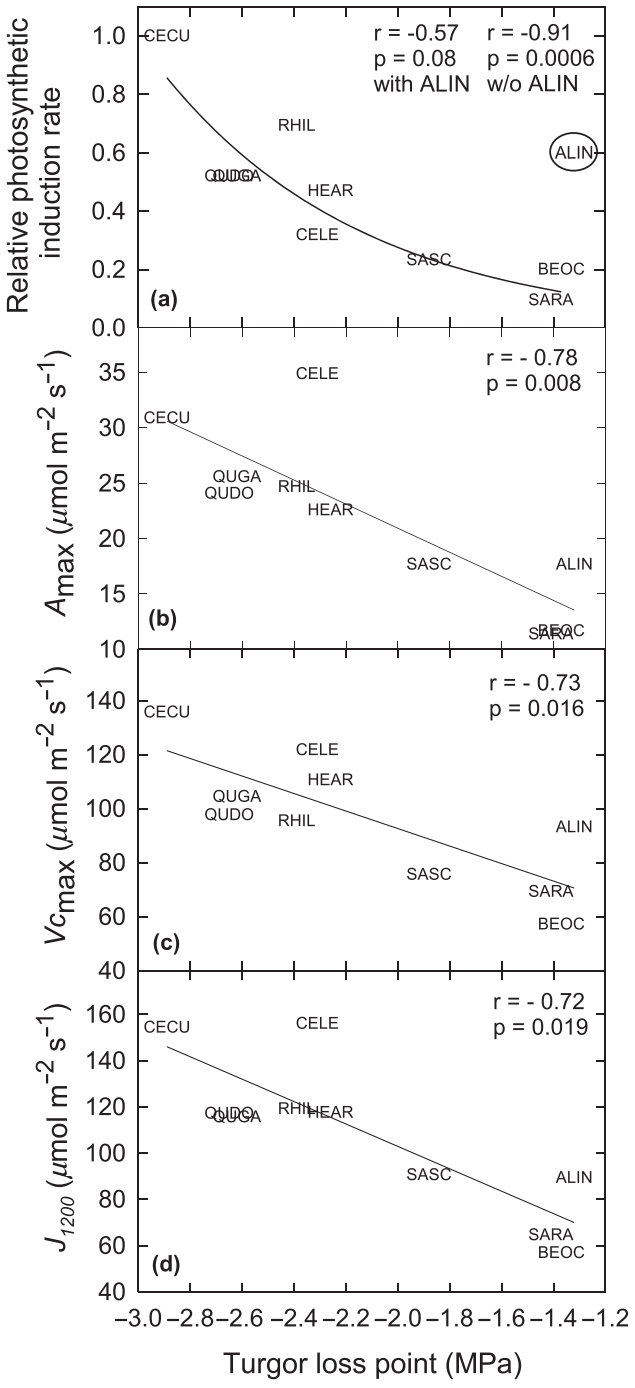

Figure 5. Photosynthetic gas exchange parameters in relation to leaf water potential at the turgor loss point. More negative values of the turgor loss point have been associated with more anisohydric stomatal regulation of leaf water potential. (a) Relative rate of light-induced photosynthetic induction. Note Spearman correlation coefficients with and without inclusion of data for ALIN owing to the presence of nodulated roots (see text). Curve fitted without ALIN. (b) Maximum photosynthetic rate estimated from A–C_i curves. (c) Maximum rate of carboxylation. (d) Maximum rate of electron transport at photosynthetically active radiation = 1200 μmol m^{-2} s^{-1}. See Table 1 for species abbreviations.

to that of *B. occidentalis* and *S. racemosa* in contrast to the pattern observed for activation of photosynthesis (Fig. 5a). The time required for complete induction of photosynthesis upon illumination of dark-adapted leaves decreased sharply with increasing N_{area} (Fig. 6a), which was highest in the most anisohydric species (Supporting Information Fig. S2b), and species values of A_{max} increased more than twofold from the lowest to highest values of N_{area} observed (Fig. 6b).

Rates of light-induced stomatal opening and induction of photosynthesis were compared in terms of half-times ($t_{50\ gs}$ and $t_{50\ A}$, respectively) to eliminate potential impacts of autocorrelation between absolute induction rates and maximum quasi--steady-state values of g_s and A (Fig. 7). When data for *A. incana* were excluded from the analysis because of

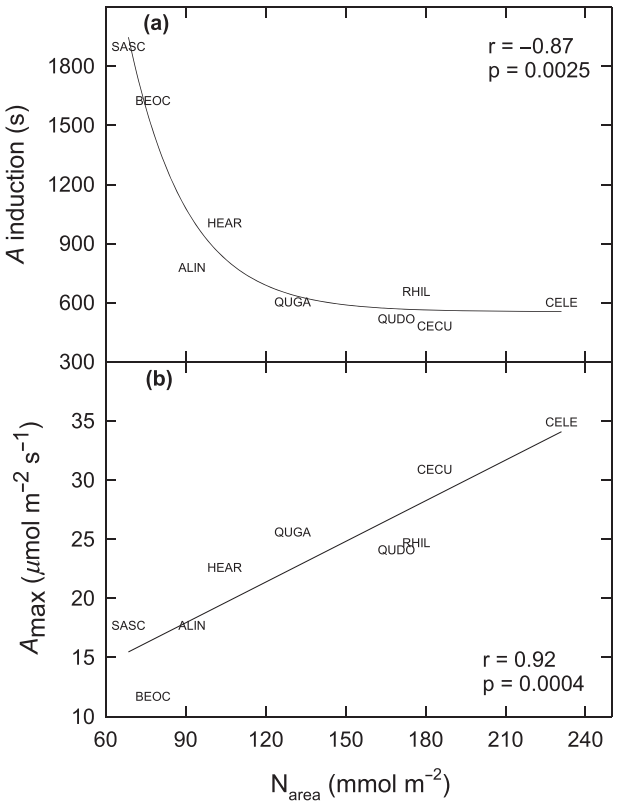

Figure 6. Leaf nitrogen content per unit area (N_{area}) in relation to (a) time required for complete light-induced activation of photosynthesis and (b) maximum CO_2-saturated rate of photosynthesis. See Table 1 for species abbreviations.

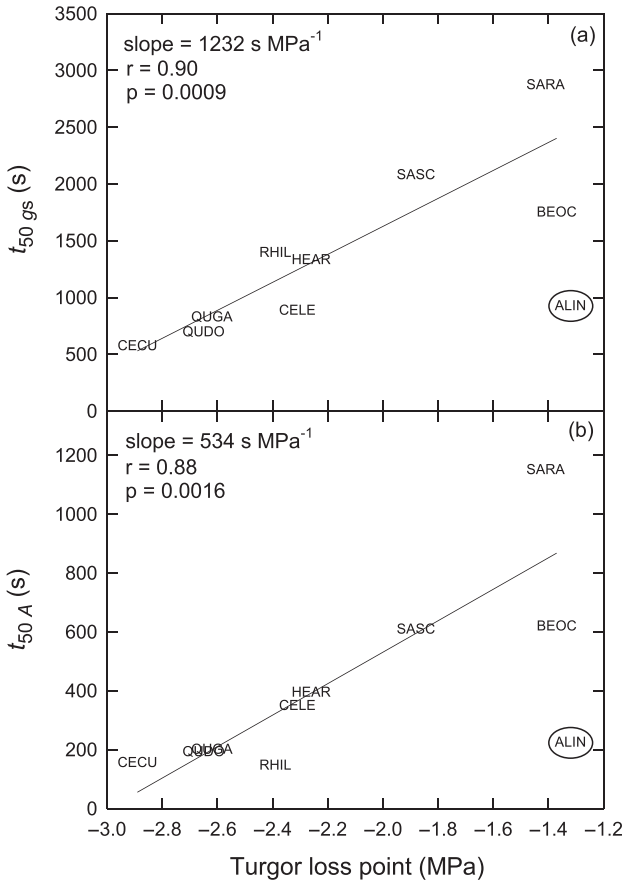

Figure 7. Half-times for light-induced stomatal opening ($t_{50\ gs}$) and activation of photosynthesis ($t_{50\ A}$) in relation to leaf water potential at the turgor loss point. More negative values of the turgor loss point have been associated with more anisohydric stomatal regulation of leaf water potential. Spearman correlation coefficients and regression lines do not include data for ALIN (circled, see text for details). See Table 1 for species abbreviations.

its root nodulation and higher leaf N content per dry mass compared with that of the two other species with similar turgor loss points, these half-times increased in a nearly linear fashion with increasing isohydry. Without *A. incana*, $t_{50\ gs}$ (Fig. 7a) and $t_{50\ A}$ (Fig. 7b) were about 5 and 14 times longer, respectively, in the species with the least negative leaf turgor loss points than in the species with the most negative turgor loss point (*C. cuneatus*). When data for *A. incana* were included in the analyses, correlations were weaker (r = 0.73), but still significant (P = 0.016). Overall, $t_{50\ A}$ was substantially smaller than $t_{50\ gs}$, indicating initially greater and then progressively diminishing stomatal limitation of photosynthesis upon illumination of dark-adapted leaves. A plot of $t_{50\ A}$ against $t_{50\ gs}$ indicated close coordination of the two variables within species and across a spectrum of isohydry to anisohydry (Fig. 8). The slope of about 0.4 s s^{-1} implied differences in the dynamics of intrinsic WUE during light-induced stomatal opening across this spectrum (Supporting Information Fig. S3).

Intrinsic WUE (A/g_s), measured upon completion of light-induced stomatal opening and activation of photosynthesis, was about two times greater in the most isohydric species studied than in the most anisohydric species studied (Fig. 9a). Species values of A/g_s were positively correlated with time-integrated estimates of intrinsic WUE based on leaf $\delta^{13}C$ values (Fig. 9b). Scaling of quasi-steady-state A with g_s was similar across species and indicated greater relative stomatal constraints on photosynthesis with increasing isohydry, consistent with the intrinsic WUE data (Fig. 10).

DISCUSSION

Anisohydric species have been shown to keep their stomata partly open and maintain photosynthetic gas exchange over a broader range of plant water status during soil drying, compared with isohydric species (e.g. West *et al.* 2007; Klein 2014; Martínez-Vilalta *et al.* 2014). Using well-irrigated plants, we found pronounced trends in dynamic and quasi-steady-state regulation of photosynthetic gas exchange in 10 diverse woody species identified as occupying different operating positions along a continuum of isohydry to anisohydry.

Consistent with our predictions, rates of light-induced stomatal opening and activation of photosynthesis increased with increasing anisohydry as did quasi-steady-state operating stomatal conductance and maximum photosynthetic rate. Intrinsic WUE decreased with increasing anisohydry, indicating

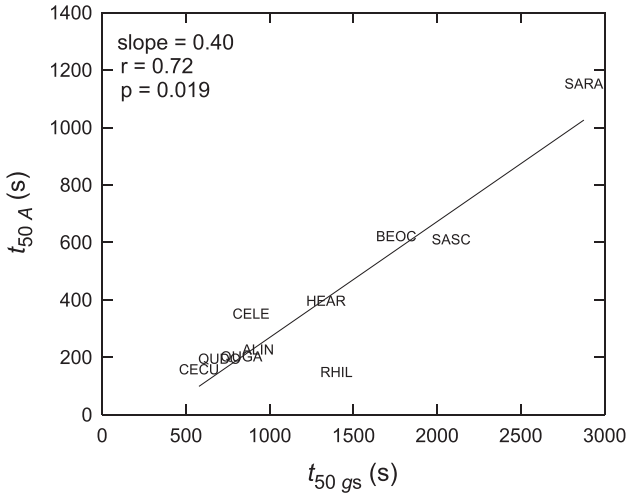

Figure 8. Species' time constants for light-induced activation of photosynthesis ($t_{50\ A}$) in relation to time constants for light-induced stomatal opening ($t_{50\ gs}$). See Table 1 for species abbreviations.

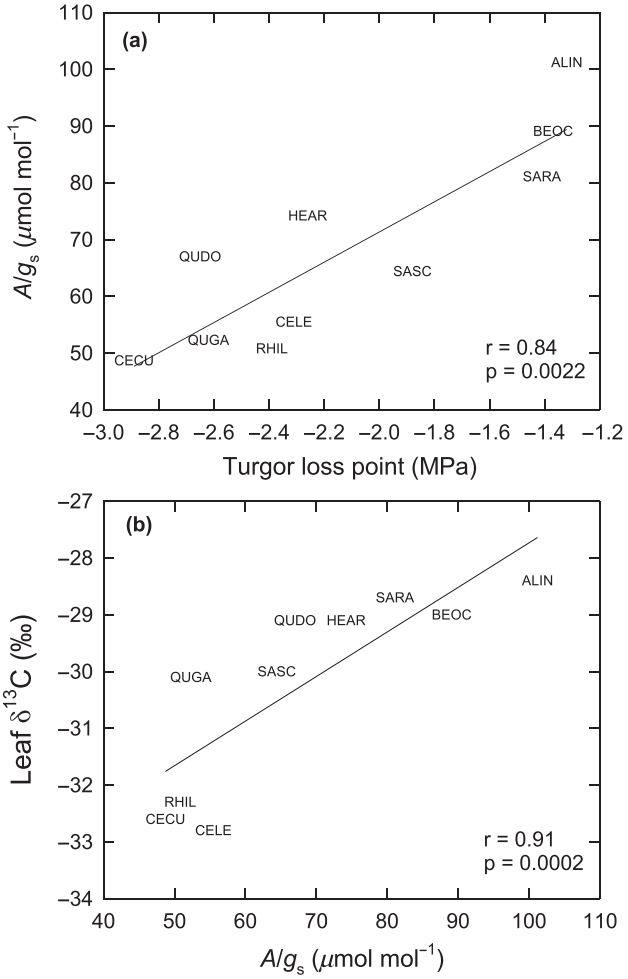

Figure 9. (a) Leaf water potential at the turgor loss point in relation to intrinsic water-use efficiency (A/g_s) after completion of light-induced activation of photosynthesis and stomatal opening. More negative values of the turgor loss point have been associated with more anisohydric stomatal regulation of leaf water potential. (b) Leaf stable carbon isotope ratios in relation to intrinsic water-use efficiency. See Table 1 for species abbreviations.

reduced relative stomatal limitation of photosynthesis. Kinetics of stomatal opening and activation of photosynthesis were closely coordinated across a continuum of isohydry to anisohydry as indicated by a linear relationship between species' half-times for light-induced stomatal opening and activation of photosynthesis. Trends in photosynthetic properties with increasing anisohydry were also associated with parallel trends in leaf nitrogen content per unit area. In comparisons between functional traits, species rankings were highly consistent, leading to species-independent scaling relationships over the range of anisohydry observed. Conducting the study under relatively uniform conditions of minimal water stress in a greenhouse common-garden-type situation likely contributed to our ability to identify these trends in inherent functional traits along a spectrum of isohydry to anisohydry.

Stomatal kinetics and maximum conductance

Maximum g_s in both isohydric and anisohydric species appears to be governed largely by leaf and guard cell turgor under a broad range of conditions (Buckley 2005; Rodriguez-Dominguez *et al.* 2016). Consistent with this, species' values of $g_{s\ op}$ in our study increased about fourfold over a 1.1-MPa range of increasing maximum leaf turgor with increasing anisohydry. The maximum rate of light-induced stomatal opening increased 12-fold over the same range of species leaf turgor values, but it is unclear whether species' differences in stomatal kinetics were driven by leaf turgor *per se*. Most studies have focused on steady-state rather than dynamic stomatal responses to changing environmental variables. The relatively few studies that have assessed stomatal kinetics have mostly done so in the context of impacts of sunflecks on understorey vegetation (Tinoco-Ojanguren & Pearcy 1993; Wong *et al.* 2012).

Recent studies on a broader array of woody and herbaceous species have emphasized the role of guard cell shape and size, stomatal density, leaf hydraulics and other attributes in determining the rapidity of stomatal responses (Drake *et al.* 2013; Lawson & Blatt 2014; Martins *et al.* 2016; McAusland *et al.* 2016). Faster kinetics have been attributed to higher stomatal density and smaller guard cell size and therefore greater surface area-to-volume ratio, which presumably facilitates solute exchange with neighbouring cells (Lawson & Blatt 2014). Some studies have shown positive correlations between stomatal density and LMA within and among species (Gratani *et al.* 2006; Dunbar-Co *et al.* 2009; Brodribb *et al.* 2013). In the present study, species' values of LMA increased with increasing anisohydry ($P = 0.03$; Supporting Information Fig. S2a), and there was a marginally significant ($P = 0.07$) positive relationship between LMA and $(dg_s/dt)_{max}$. The preceding relationships imply that faster stomatal kinetics in anisohydric species may result from a combination of a higher density of smaller stomata and higher bulk leaf turgor than in isohydric species.

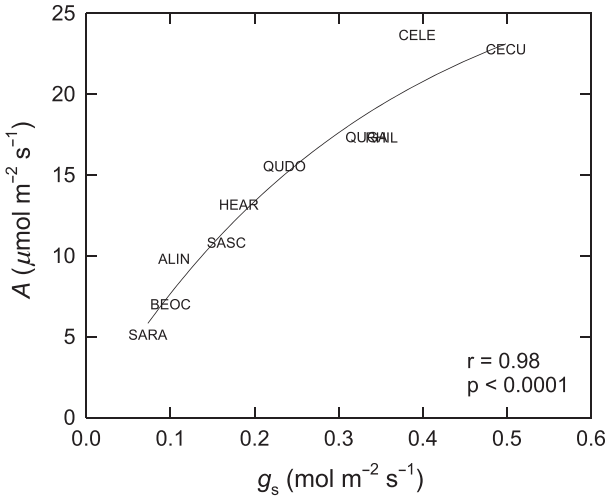

Figure 10. Relationship between net photosynthesis and stomatal conductance at the times A/g_s was measured in Fig. 9a. See Table 1 for species abbreviations.

Coordination of photosynthetic and stomatal traits

Although leaf turgor and stomatal size and density likely played a dominant role in determining dynamic and steady-state stomatal behaviour, faster rates of light-induced activation of photosynthesis and higher A_{max} with increasing anisohydry appeared to be at least partly governed by leaf N content on an area basis. We expected leaf-area-based photosynthetic properties to be more closely associated with N_{area} than with N content on a dry weight basis because of the large variation in LMA among species (Supporting Information Fig. S2a). Additionally, our proxy for anisohydry, Ψ_{TLP}, was significantly correlated with N_{area} (Supporting Information Fig. S2b), but not with leaf N on a dry weight basis ($P = 0.7$). The time required for completion of light-induced activation of photosynthesis decreased with increasing N_{area} in a similar fashion across species, and there appeared to be a threshold minimum value of N_{area} below which species' induction times began to increase exponentially (Fig. 6a). However, other metrics of maximal or near-maximal rates of light-induced activation of photosynthesis showed kinetics in *A. incana* to be about three times faster than that in *B. occidentalis* and *Salix scouleriana*, similarly isohydric species with similar N_{area} (Figs 5a, 6b & 7b). It is unknown whether the apparent presence of N-fixing bacteria in roots of *A. incana* contributed to its faster kinetics of photosynthetic induction than in other species with roughly similar or greater N_{area}. In addition to the potential influence of N_{area} on photosynthetic induction kinetics, the close coordination between the kinetics of stomatal and photosynthetic induction across species (Fig. 8) is suggestive of a direct role of g_s in regulating rates of Rubisco activation through its effects on C_i (Mott & Woodrow 1993). Consistent with this, $t_{50\ A}$ was inversely correlated with both $g_{s\ dark}$ ($P = 0.016$) and $g_{s\ op}$ ($P = 0.010$). However, $t_{50\ A}$ was not significantly correlated ($P \geq 0.19$) with various measures of post-illumination C_i (data not shown).

Intrinsic WUE, as estimated by quasi-steady-state A/g_s and leaf $\delta^{13}C$ values, decreased with increasing N_{area} (Supporting Information Fig. S4). Other studies have reported increases in intrinsic WUE with increasing N_{area} within species when N-induced gains in A_{max} outweigh concomitant adjustments in g_s that would increase or maintain relative stomatal limitations on photosynthesis (e.g. Clearwater & Meinzer 2001; Adams *et al.* 2016). The contrasting pattern observed here is suggestive of anisohydric species prioritizing carbon gain over WUE when soil water availability is adequate (Wolf *et al.* 2016).

'Fast' and 'slow' traits and trade-offs along a spectrum of isohydry to anisohydry

Reich (2014) expanded the concept of a carbon-based and nutrient-based leaf economics spectrum (Wright *et al.* 2004) to include water as well as stems, roots and whole plants. He proposed that biophysical constraints on possible combinations of traits result in multiple trade-offs among them, causing species to operate at different positions along a spectrum of fast to slow strategies in terms of rates of resource acquisition and use. Consistent with a 'fast–slow' plant economics spectrum, we previously found that increasingly negative leaf Ψ_{TLP} among species served as a proxy for increasing anisohydry and the ability to acquire water to sustain photosynthetic gas exchange over an increasingly large water potential landscape or 'hydroscape' (Meinzer *et al.* 2016). Thus, isohydry versus anisohydry represents a continuum of whole-plant strategies for the acquisition and use of water as well as acquisition of carbon as reflected in the stringency of stomatal control of gas exchange and plant water status.

In the current study, we found trade-offs of faster kinetics and higher rates of photosynthetic gas exchange against higher relative carbon investment in leaves and stems of anisohydric plants. LMA was roughly twice as great in the species with the most negative values of Ψ_{TLP}, and therefore the fastest gas exchange kinetics and rates, than in the species with the least negative values of Ψ_{TLP} (Supporting Information Fig. S2). Similarly, wood density increased from 0.24 to 0.84 g cm^{-3} with decreasing Ψ_{TLP} ($P = 0.002$, Supporting Information Fig. S5). Greater wood density is generally associated with lower capacitance (Pratt *et al.* 2007a; Scholz *et al.* 2007; Meinzer *et al.* 2008), implying a requirement for faster stomatal kinetics to buffer transpiration-induced changes in xylem tension in anisohydric species. Greater wood density is also frequently, but not universally, correlated with lower hydraulic conductivity (Santiago *et al.* 2004; Meinzer *et al.* 2008) and greater xylem resistance to drought-induced embolism (Hacke *et al.* 2001; Pratt *et al.* 2007a; Bucci *et al.* 2006). Consistent with this, published values of stem xylem pressure at 50% loss of hydraulic conductivity (P_{50}) for field-grown plants of the most extreme anisohydric and isohydric species in our study range from about −8.5 MPa in *C. cuneatus* (Pratt *et al.* 2007b) to −1.4 MPa in *B. occidentalis* (Sperry & Saliendra 1994). Maintenance of high rates of leaf gas exchange in anisohydric species despite lower xylem hydraulic conductivity may be facilitated by lower ratios of leaf area to

xylem area than in isohydric species, but this was not investigated in the present study. Higher leaf solute content with increasing anisohydry also implies an energy trade-off for being able to maintain turgor and sustain photosynthetic gas exchange over a broader range of leaf Ψ than in isohydric species. The preceding and other differences in relative carbon and energy allocation per unit leaf area and stem volume between isohydric and anisohydric species point to an overall greater investment of photosynthate per unit leaf area displayed in anisohydric species. However, this allocation pattern may not necessarily result in lower growth rates and whole-plant hydraulic conductance in anisohydric species when soil water availability is adequate (Mitchell *et al.* 2013).

CONCLUSION

Our results are consistent with previous evidence that a simple and easily determined plant trait, the bulk leaf osmotic potential at turgor loss, can serve as a robust proxy for multiple and more complex traits governing plant responses to drought (Bartlett *et al.* 2012, 2016; Maréchaux *et al.* 2015). Use of Ψ_{TLP} as a proxy for an array of other plant functional traits may simplify efforts to model species' responses to different drought scenarios. The complexes of coordinated traits observed here and elsewhere have led to the hypothesis that during prolonged drought, anisohydric species are more likely to die of hydraulic failure and isohydric species of carbon starvation owing to differences in stringency of stomatal control of gas exchange (McDowell *et al.* 2008). However, given that isohydry versus anisohydry represents a continuum of strategies, it may be difficult to predict species-specific mechanisms of drought-induced mortality even if species' positions along the continuum can be quantified using proxies such as leaf Ψ_{TLP}. Moreover, if phloem transport failure is considered as an additional potential mechanism of drought-induced mortality (McDowell *et al.* 2011; Mencuccini *et al.* 2015), associating a specific mortality mechanism with a species' degree of anisohydry becomes more complex and context dependent (McDowell *et al.* 2011; Anderegg *et al.* 2015; Mencuccini *et al.* 2015).

ACKNOWLEDGMENTS

This work was supported in part by NSF grant IOS 11-46746 and an NSF Graduate Research Fellowship to D.E.M. We are grateful to the OSU Greenhouse Operations staff members for their assistance with the maintenance of our plant material.

REFERENCES

Adams M.A., Turnbull T.A., Sprent J.I. & Buchmann N. (2016) Legumes are different: leaf nitrogen, photosynthesis, and water use efficiency. *Proceedings of the National Academy of Sciences USA* **113**, 4098–4103.

Anderegg W.R.L., Berry J.A., Smith D.D., Sperry J.S., Anderegg L.D.L. & Field C.B. (2012) The roles of hydraulic and carbon stress in a widespread climate-induced forest die-off. *Proceedings of the National Academy of Sciences USA* **109**, 233–237.

Anderegg W.R.L., Hicke J.A., Fisher R.A., Allen C.D., Aukema J., Bentz B., … Zeppel M. (2015) Tree mortality from drought, insects and their interactions in a changing climate. *New Phytologist* **208**, 674–683.

Bartlett M.K., Scoffoni C. & Sack L. (2012) The determinants of leaf turgor loss point and prediction of drought tolerance of species biomes: a global meta-analysis. *Ecology Letters* **15**, 393–405.

Bartlett M.K., Klein T., Jansen S., Choat B. & Sack L. (2016) The correlations and sequence of plant stomatal, hydraulic and wilting responses to drought. *Proceedings of the National Academy of Sciences USA* **113**, 13098–13103.

Brodribb T.J., Jordan G.J. & Carpenter R.J. (2013) Unified changes in cell size permit coordinated leaf evolution. *New Phytologist* **199**, 559–570.

Bucci S.J., Goldstein G., Meinzer F.C., Scholz F.G., Franco A.C. & Bustamante M. (2004) Functional convergence in hydraulic architecture and water relations of tropical savanna trees: from leaf to whole plant. *Tree Physiology* **24**, 891–899.

Bucci S.J., Scholz F.G., Goldstein G., Meinzer F.C., Franco A.C., Campanello P.I., … Miralles-Wilhelm F. (2006) Nutrient availability constrains the hydraulic architecture and water relations of savanna trees. *Plant, Cell and Environment* **29**, 2153–2167.

Bucci S.J., Scholz F.G., Peschiutta M.L., Arias N.S., Meinzer F.C. & Goldstein G. (2013) The stem xylem of Patagonian shrubs operates far from the point of catastrophic dysfunction and is additionally protected from drought-induced embolism by leaves and roots. *Plant, Cell and Environment* **36**, 2163–2174.

Buckley T.N. (2005) The control of stomata by water balance. *New Phytologist* **168**, 275–292.

Clearwater M.J. & Meinzer F.C. (2001) Relationships between hydraulic architecture and leaf photosynthetic capacity in nitrogen-fertilized *Eucalyptus grandis* trees. *Tree Physiology* **21**, 683–690.

Drake P.L., Froend R.H. & Franks P.J. (2013) Smaller, faster stomata: scaling of stomatal size, rate of response, and stomatal conductance. *Journal of Experimental Botany* **64**, 495–505.

Dunbar-Co S., Sporck M.J. & Sack L. (2009) Leaf trait diversification and design in seven rare taxa of the Hawaiian *Plantago* radiation. *International Journal of Plant Sciences* **170**, 61–75.

Ewers B.E., Mackay D.S. & Samanta S. (2007) Interannual consistency in canopy stomatal conductance control of leaf water potential across seven tree species. *Tree Physiology* **27**, 11–24.

Franks P.J., Drake P.L. & Froend R.H. (2007) Anisohydric but isohydrodynamic: seasonally constant plant water potential gradient explained by a stomatal control mechanism incorporating variable plant hydraulic conductance. *Plant, Cell and Environment* **30**, 19–30.

Garcia-Forner N., Biel C., Savé R. & Martinez-Vilalta J. (2016a) Isohydric species are not necessarily more carbon limited than anisohydric species during drought. *Tree Physiology* https://doi.org/10.1093/treephys/tpw109.

Garcia-Forner N., Adams H.D., Sevanto S., Collins A.D., Dickman L.T., Hudson P.J., … McDowell N.G. (2016b) Responses of two semi-arid conifer tree species to reduced precipitation and warming reveal new perspectives for stomatal regulation. *Plant, Cell and Environment* **39**, 38–49.

Gratani L., Covone F. & Larcher W. (2006) Leaf plasticity in response to light in three evergreen species of the Mediterranean maquis. *Trees* **20**, 549–558.

Hacke U.G., Sperry J.S., Pockman W.T., Davis S.D. & McCulloh K.A. (2001) Trends in wood density and structure are linked to prevention of xylem implosion by negative pressure. *Oecologia* **126**, 457–461.

Hubbard R.M., Ryan M.G., Stiller V. & Sperry J.S. (2001) Stomatal conductance and photosynthesis vary linearly with plant hydraulic conductance in ponderosa pine. *Plant, Cell & Environment* **24**, 113–121.

Klein T. (2014) The variability of stomatal sensitivity to leaf water potential across tree species indicates a continuum between isohydric and anisohydric behaviors. *Functional Ecology* **28**, 1313–1320.

Lawson T. & Blatt M.R. (2014) Stomatal size, speed, and responsiveness impact on photosynthesis and water use efficiency. *Plant Physiology* **164**, 1556–1570.

Maréchaux I., Bartlett M.K., Sack L., Baraloto C., Engel J., Joetzjer E., et al. (2015) Drought tolerance as predicted by leaf water potential at turgor loss point varies strongly across species within an Amazonian forest. *Functional Ecology* **29**, 1268–1277.

Martínez-Vilalta J., Poyatos R., Aguade D., Retana J. & Mencuccini M. (2014) A new look at water transport regulation in plants. *New Phytologist* **204**, 105–115.

Martínez-Vilalta J. & Garcia-Forner N. (2016) Water potential regulation, stomatal behavior and hydraulic transport under drought: deconstructing the iso/anisohydric concept. *Plant, Cell & Environment*. https://doi.org/10.1111/pce.12846.

Martins S.C., McAdam S.A.M., Deans R.M., DaMatta F.M. & Brodribb T.J. (2016) Stomatal dynamics are limited by leaf hydraulics in ferns and conifers:

results from simultaneous measurements of liquid and vapor fluxes in leaves. *Plant, Cell and Environment* **39**, 694–705.
McAusland L., Vialet-Chabrand S., Davey P., Baker N.R., Brendel O. & Lawson T. (2016) Effects of kinetics of light-induced stomatal responses on photosynthesis and water-use efficiency. *New Phytologist* **211**, 1209–1220.
McDowell N.G., Pockman W.T., Allen C.D., Breshears D.D., Cobb N., Kolb T., … Yepez E.A. (2008) Mechanisms of plant survival and mortality during drought: why do some plants survive while others succumb to drought? *New Phytologist* **178**, 719–739.
McDowell N.G., Beerling D.J., Breshears D.D., Fisher R.A., Raffa K.F. & Stitt M. (2011) The interdependence of mechanisms underlying climate-driven vegetation mortality. *Trends in Ecology and Evolution* **26**, 523–532.
Meinzer F.C. (2002) Coordination of vapor and liquid phase water transport properties in plants. *Plant, Cell and Environment* **25**, 265–274.
Meinzer F.C. & Grantz D.A. (1990) Stomatal and hydraulic conductance in growing sugarcane: stomatal adjustment to water transport capacity. *Plant, Cell & Environment* **13**, 383–388.
Meinzer F.C., Campanello P.I., Domec J.-C., Gatti M.G., Goldstein G., Villalobos-Vega R. & Woodruff D.R. (2008) Constraints on physiological function associated with branch architecture and wood density in tropical forest trees. *Tree Physiology* **28**, 1609–1617.
Meinzer F.C., Johnson D.M., Lachenbruch B., McCulloh K.A. & Woodruff D.R. (2009) Xylem hydraulic safety margins in woody plants: coordination of stomatal control of xylem tension with hydraulic capacitance. *Functional Ecology* **23**, 922–930.
Meinzer F.C., Woodruff D.R., Marias D.E., Smith D.D., McCulloh K.A., Howard A.R. & Magedman A.L. (2016) Mapping 'hydroscapes' along the iso- to anisohydric continuum of stomatal regulation of plant water status. *Ecology Letters* **19**, 1343–1352.
Mencuccini M., Minunno F., Salmon Y., Martínez-Vilalta J. & Holtta T. (2015) Coordination of physiological traits involved in drought-induced mortality of woody plants. *New Phytologist* **208**, 396–409.
Mitchell P.J., O'Grady A.P., Tissue D.T., White D.A., Ottenschlaeger M.L. & Pinkard E.A. (2013) Drought response strategies define the relative contributions of hydraulic dysfunction and carbohydrate depletion during tree mortality. *New Phytologist* **197**, 862–872.
Mott K.A. & Woodrow I.E. (1993) Effects of O_2 and CO_2 on nonsteady-state photosynthesis. *Plant Physiology* **102**, 859–866.
Pratt R.B., Jacobsen A.L., Ewers F.W. & Davis S.D. (2007a) Relationships among xylem water transport, biomechanics and storage in stems and roots of nine Rhamnaceae species of the California chaparral. *New Phytologist* **174**, 787–798.
Pratt R.B., Jacobsen A.L., Golgotiu K.A., Sperry J.S., Ewers F.W. & Davis S.D. (2007b) Life history type and water stress tolerance in nine California chaparral species (Rhamnaceae). *Ecological Monographs* **77**, 239–253.
Raschke K. (1975) Stomatal action. *Annual Review of Plant Physiology* **26**, 309–340.
Reich P.B. (2014) The world-wide 'fast–slow' plant economics spectrum: a traits manifesto. *Journal of Ecology* **102**, 275–301.
Rodriguez-Dominguez C.M., Buckley T.N., Egea G., de Cires A., Hernandez-Santana V., Martorell S. & Diaz-Espejo A. (2016) Most stomatal closure in woody species under moderate drought can be explained by stomatal responses to leaf turgor. *Plant, Cell and Environment* **39**, 2014–2026.
Santiago L.S., Goldstein G., Meinzer F.C., Fisher J.B., Machado K., Woodruff D. & Jones T. (2004) Leaf photosynthetic traits scale with hydraulic conductivity and wood density in Panamanian forest canopy trees. *Oecologia* **140**, 543–550.
Scholz F.G., Bucci S.J., Goldstein G., Meinzer F.C., Franco A.C. & Miralles-Wilhelm F. (2007) Biophysical properties and functional significance of stem water storage tissues in neotropical savanna trees. *Plant, Cell and Environment* **30**, 236–248.
Sharkey T.D., Bernacchi C.J., Farquhar G.D. & Singsaas E.L. (2007) Fitting photosynthetic carbon dioxide response curves for C_3 leaves. *Plant, Cell and Environment* **30**, 1035–1040.
Skelton R.P., West A.G. & Dawson T.E. (2015) Predicting plant vulnerability to drought in biodiverse regions using functional traits. *Proceedings of the National Academy of Sciences USA* **112**, 5744–5749.
Sparks J.P. & Black R.A. (1999) Regulation of water loss in populations of *Populus trichocarpa*: the role of stomatal control in preventing xylem cavitation. *Tree Physiology* **19**, 453–459.
Sperry J.S. & Saliendra N.Z. (1994) Intra- and inter-plant variation in xylem cavitation in *Betula occidentalis*. *Plant, Cell and Environment* **17**, 1233–1241.
Tardieu F. & Simonneau T. (1998) Variability of species among stomatal control under fluctuating soil water status and evaporative demand: modeling isohydric and anisohydric behaviours. *Journal of Experimental Botany* **49**, 419–432.
Tinoco-Ojanguren C. & Pearcy R.W. (1993) Stomatal dynamics and its importance to carbon gain in two rainforest *Piper* species. *Oecologia* **94**, 395–402.
Vogt U.K. (2001) Hydraulic vulnerability, vessel refilling, and seasonal courses of stem water potential of *Sorbus aucuparia* L. and *Sambucus nigra* L. *Journal of Experimental Botany* **52**, 1527–1536.
West A.G., Hultine K.R., Jackson T.L. & Ehleringer J.R. (2007) Differential summer water use by *Pinus edulis* and *Juniperus osteosperma* reflects contrasting hydraulic characteristics. *Tree Physiology* **27**, 1711–1720.
Wolf A., Anderegg W.R.L. & Pacala S.W. (2016) Optimal stomatal behavior with competition for water and risk of hydraulic impairment. *Proceedings of the National Academy of Sciences USA* **113**, E7222–E7230.
Wong S.L., Chen C.W., Huang H.W. & Weng J.H. (2012) Using combined measurements for comparison of light induction of stomatal conductance, electron transport rate and CO_2 fixation in woody and fern species adapted to different light regimes. *Tree Physiology* **32**, 535–544.
Wright I.J., Reich P.B., Westoby M., Ackerly D.D., Baruch Z., Bongers F., … Villar R. (2004) The worldwide leaf economics spectrum. *Nature* **428**, 821–827.

Received 1 February 2017; received in revised form 4 April 2017; accepted for publication 10 April 2017

SUPPORTING INFORMATION

Additional Supporting Information may be found online in the supporting information tab for this article.

Table S1. Mean plant heights, crown diameters and basal stem diameters (±SD).
Table S2. Species' means and standard errors (n = 3–5) of variables plotted in Figs 2-10.
Figure S1. Sample time courses of light-induced activation of photosynthesis in dark-adapted leaves of two woody species representing different operating points along a continuum of isohydry to anisohydry. Once the ratio of the CO_2 assimilation rate (A, μmol m^{-2} s^{-1}) to the intercellular CO_2 concentration (C_i, μmol mol^{-1}) becomes constant or nearly constant, photosynthesis is considered to be fully activated. Leaves were illuminated at time = 0. Based on their leaf turgor loss points, *Ceanothus cuneatus* is more anisohydric than *Salix scouleriana*.
Figure S2. Leaf mass per area (a) and leaf nitrogen content per unit area (b) in relation to leaf water potential at the turgor loss point for 10 woody species. See Table 1 in text for species codes.
Figure S3. Sample time courses of intrinsic water-use efficiency (A/g_s) upon illumination of dark-adapted leaves at time = 0. Based on their leaf turgor loss points, *Ceanothus cuneatus* is more anisohydric than *Betula occidentalis*.
Figure S4. Relationships between two measures of intrinsic water-use efficiency and leaf nitrogen content per unit area (N_{area}). (a) The ratio of net CO_2 assimilation to stomatal conductance and (b) leaf tissue stable carbon isotope ratio.
Figure S5. Relationship between stem wood density and leaf water potential at the turgor loss point for 10 woody species representing different operating points along a continuum of isohydry to anisohydry. See Table 1 in text for species codes.